American Journal of Biomedical and Life Sciences
2024, Vol. 12, No. 3, pp. 30-48
https://doi.org/10.11648/j.ajbls.20241203.12

Research Article

Reversal of P-glycoprotein Mediated Multidrug Resistance in MCF-7/R Cancer Cells by Esculetin Derivatives: Experimental and MD Simulation Studies

Navanath Kumbhar[1], Neelofar Khan[2], Rohit Bavi[3, 4], Sagar Barage[5], Ayesha Khan[2, *]

[1]Department of Biotechnology, Medical Information Management, Shivaji University, Kolhapur, India
[2]Department of Chemistry, Savitribai Phule Pune University, Pune, India
[3]Department of Biomedical Engineering, China Pharmaceutical University, Nanjing, China
[4]School of Chemical Science, Punyashlok Ahilyadevi Holkar Solapur University, Solapur, India
[5]Amity Institute of Biotechnology, Amity University, Mumbai, India

Abstract

Coumarins of natural origin have been explored as potential inhibitors of P-glycoprotein (P-gp). Esculetin which belongs to the class of coumarin has been derivatized with known hydrazine pharmacophores viz; benzoyl hydrazine (BH), isonicotinyl hydrazine (INH), and hydrazino benzoic acid. The homology modeling approach was used to predict the three-dimensional structure of human P-gp. An *in-silico* study has been performed for the structural insight into the molecular mechanism of P-gp inhibition of the esculetin derivatives by molecular docking (MD) and simulation studies. The cell cytotoxic activities of the synthesized compounds were evaluated using in-vitro studies. The sublines resistant doxorubicin (MCF-7/R) were generated and the activities of P-gp proteins were estimated using fluorescent dye accumulation assays. The E-BH showed promising P-gp inhibitory activity and cell cytotoxicity against MCF7 and MCF7/R (resistant) breast cancer cell lines. In line with experimental observations, the E-BH (Esculetin benzoyl hydrazine) has yielded the lowest energy stable complex with P-gp and is stabilized by intermolecular hydrogen bonding and more hydrophobic interactions during 100 ns of simulation. This suggested that the activity of P-gp is probably controlled by hydrophobic interactions. Performed experimental and computational studies has helped to elucidate the mechanism of P-gp inhibition by E-BH. Thus, amongst the three derivatives; E-BH exhibits greater efficacy in blocking the efflux mechanism.

Keywords

Esculetin Hydrazine Derivatives, Pgp Inhibitors, Homology Modeling, Docking, Molecular Dynamics Simulation

[*]Corresponding author: Ayesha.khan@unipune.ac.in (Ayesha Khan)

Received: 1 July 2024; **Accepted:** 29 July 2024; **Published:** 27 August 2024

1. Introduction

The P-glycoprotein (P-gp) or ABCB1 is an ATP binding cassette (ABC) transporter and one of the widely studied mediators of drug efflux-based multidrug resistance (MDR) in cancer [1-3] P-gp is known to bind to the structurally diverse size of molecules (100 to 4000 daltons) and actively extrude them across the plasma membrane of various types of cells. This leads to an increase in cellular drug resistance toward the chemotherapeutic agents. Thus P-gp acts as a prominent target for designing effective anti-cancer drugs. [4, 5] Considering the immense role of P-gp in drug efflux mediated multidrug resistance (MDR) in cancer; many studies have been performed to discover the structure, dynamics, and functions of human P-gps. [5, 6-14] Understanding the conformational flexibility and P-gp-drug interactions during the translocation process is a crucial step towards the designing of potent and selective inhibitors against the P-gp. This may initiate the treatment of MDR in cancer subtypes along with neurological diseases including Alzheimer's, Parkinson and Epilepsy. [7, 9, 15-19] Owing to the dynamic nature of P-gps, the molecular dynamics simulation is one of the best approaches to study the conformational behavior of P-gp, especially by evaluating the influence of the surrounding environment. [8, 16, 20-22] Combinatorial chemistry and structure-activity relationship approaches have been used in the third generation P-gp blockers to generate compounds such as zosuquidar (LY335979), elacridar (GF120918), etc with antagonism function in the range 20-100 nM.

The 3D-QSAR, molecular docking, and in-depth MD simulation studies have been performed to design new anti-P-gp inhibitors, locate the molecular interactions between P-gp and inhibitors, explore the conformational dynamics of P-gp, and substantiate the experimental observations. [8, 16, 22-27] Recently, all-atom MD simulation studies confirmed that the inward-facing conformations of P-gp were highly plausible in presence of an intact lipid bilayer. [21, 22, 28, 29] The computational techniques are playing a crucial role in understanding the structure, dynamics, and functions of human P-gp. The three-dimensional structure of human P-gp predicted using homology modeling is being used for further studies. [19, 23, 25, 27, 29-32]

P-gp blockers of natural origin such as flavonoids, stilbenes, and coumarins are explored as potential inhibitors. An *in-silico* study has been performed to depict the molecular interactions between various coumarin derivatives and anticancer drug (paclitaxel) with the P-gp. [33] Esculetin (6,7-dihydroxycoumarin) [1] is a coumarin derivative extracted from plants, such as *Artemesia scoparia* (Redstem Wormwood), *Artemesia capillaris* (Capillary Wormwood), *Ceratostigma willmottianum* (Chinese Plumbago), skin or trunk bark of *Cortex Fraxini* and in the leaves of *Citrus limonia* (Chinese lemon). [34] Esculetin, commonly used in folk medicine has been reported to possess various pharmacological and biochemical activities including anti-oxidant, anti-inflammatory, anti-proliferative, and anti-obesity activity. [35]

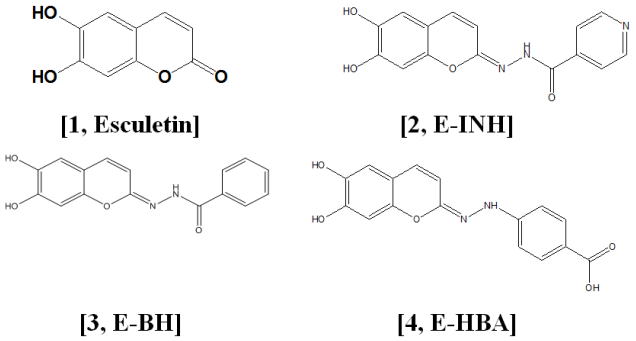

Scheme 1. *Esculetin derivatives.*

Using MDR1 transfected Madin-Darby canine kidney (MDCK-MDR1) cells expressing MDR1 phenotype and verapamil as a positive control along with six natural coumarins viz. umbelliferone, esculin, esculetin, cnidiadin, angelicin, and psoralen were evaluated. Cniadin (furanocoumarin) was capable of significantly accumulating R-123 and [^{3}H]-vinblastine ([^{3}H]-VBL), and inhibiting P-gp photolabeling in MDCK-MDR1 cells. [36] Hydrazone pharmacophores have been used extensively for derivatization and modulating pharmacological activity. [37] In the present paper, the natural coumarin has been derivatized using different hydrazine pharmacophores. Thus three different analogs of Esculetin hydrazine were synthesized, tested for their anti-P-gp activity, and further substantiated by homology modeling, molecular docking, and MD simulation studies.

The performed experimental and computational studies may prove the potential to acquire the conformational dynamics of P-gp and its catalytic inhibition mechanism. The studies will help to design new potent and selective inhibitors of P-gp using *in-vitro* and *in-silico* studies.

2. Materials and Methods

2.1. Synthesis of Esculetin Derivatives

Substituted hydrazones of coumarin possess biological activities like anti-inflammatory, antibacterial, antifungal, anticancer, antitubercular, and antioxidant. [38] Because of a wide variety of biological activity we are interested in the preparation of Hydrazone derivatives of esculetin. Esculetin was reacted with hydrazines in toluene by the Schiff base condensation method to give esculetin hydrazone derivatives. The molecular water produced in the reaction was extracted using molecular sieves. The solvents were dried thoroughly using known protocols. The esculetin hydrazone derivatives

such as esculetin-isonicotyl hydrazide (E-INH) 15, esculetin-benzoyl hydrazide (E-BH) 16 and esculetin-hydrazinobenzoic acid (E-HBA) 17 were condensed by directly reacting esculetin with isonicotyl hydrazide (INH) 12, benzoyl hydrazide (BH) 13 and hydrazinobenzoic acid (HBA) 14, respectively.

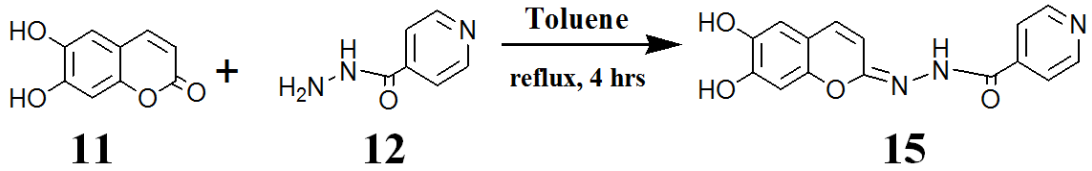

Scheme 2. Preparation of esculetin-isonicotyl hydrazide.

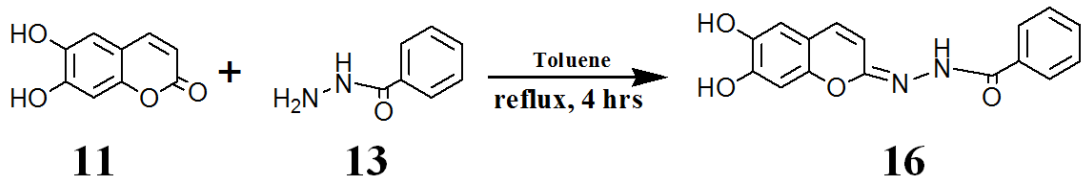

Scheme 3. Preparation of esculetin-benzoyl hydrazide.

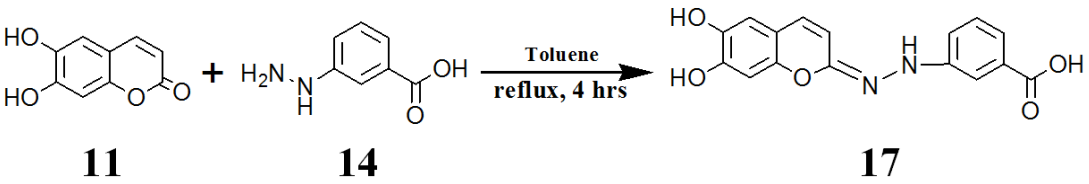

Scheme 4. Preparation of esculetin- hydrazinobenzoic acid.

2.1.1. Characterization

Fourier transform infrared spectroscopy (FTIR) measurements were recorded on Bruker Platinum ATR TENSOR- 37 spectrophotometer (Germany) in the 4000-400 cm^{-1} region at room temperature. While ^{1}H NMR was reported in Bruker Advance III HD NMR 400 MHz machine using d^{6}-DMSO as a solvent. HRMS spectra were recorded on a Bruker Impact HD UHR-TOF mass spectrometer using an ESI (Electron Spray Ionization) source. The mass spectra were recorded using the method of 50-600 mass range. The compounds were analyzed with LCMS positive ion mode by using acetonitrile/methanol as solvent.

2.1.2. HPLC Analysis of Synthesized E-BH, E-HBA and E-INH Compounds

Bruker UPLC (Thermo)-MS was used to quantify the purity of the synthesized compounds. HPLC at two wavelengths 254 nm and 290 nm using the following conditions: 1.7 µm Evo C18 100A, LC column 50 mm × 2.1 mm, solvent A of 0.1% (formic acid) water, solvent B of 0.1% (formic acid) acetonitrile was set for 40 mins using gradient elution. Esculetin used in the synthesis was purchased from Sigma Aldrich (purity > 99%). While, E-BH (% yield 18 %), E-HBA (% yield 21 %), and E-INH (% yield 16 %) column purified were analyzed by UHPLC wherein the data indicate > 95 % purity.

Note: Complete chemical characterization of the compound is reported in Figures S1-S4 in the supplementary information.

2.2. Biological Activity

2.2.1. Cell Lines, Development of Resistant Subline

MCF-7 cells (attached type monolayer culture) were maintained in RPMI 1640 medium supplemented with 10% heat-inactivated fetal bovine serum, L-glutamine, and antibiotics (Penicillin and Streptomycin). The cultures were maintained at 37 ℃ in a humidified atmosphere of 5% CO_2 in a Thermo Fischer Scientific incubator. The sublines resistant doxorubicin (MCF-7/Dox) for doxorubicin were generated as per the reference, with subsequent treatment of Dox from 10 nM to 600 nM. [39, 40] Developed sublines were tested for activities of P-gp proteins using fluorescent dye accumulation assays.

2.2.2. Anti-Proliferative Activity Assay

The proliferation activities of the esculetin derivatives were

tested on sensitive and resistant MCF-7 cell lines. [41] The test compounds were diluted with serial dilution in the 96-well microtiter plates. 1 x 10^4 cells were seeded in each well and the plates were incubated at 37 ℃ for 72 h. The control well was assigned accordingly. For the assay 20 µL of 5 mg/mL MTT solution was added to each well. The plates were incubated at 37 ℃ for 4 h. For the dissolution of formazan crystals produced by the mitochondrial enzymes from the living cells, plates were further incubated at 37 ℃ overnight. The cell proliferation inhibition was determined by measuring the optical density of the colored product at 570 nm with a Perkin Elmer (Enspire) multiplate reader.

2.2.3. Rhodamine 123 Intracellular Uptake and Efflux Assay

The cell concentrations of the Parental and resistant cell lines were adjusted to 2 x 10^6 cells/mL. The trypsinized cells were suspended in RPMI 1640 medium and 0.5 mL of the aliquots was placed in micro-centrifuge tubes. 40 µg/mL of the compounds to be tested were incubated for 10 min at 25 ℃. Rhodamine-123 (P-gp substrate) was added to the samples, and cells were incubated for 20 min at 37 ℃. After centrifugation, the cells were washed twice in 0.5 mL PBS and re-suspended in 0.5 mL PBS for the assay. The cell population was measured using flow cytometry using fluorescence. The fluorescent activities for the treated MCF-7 cell lines were calculated by comparing them with the fluorescent activities of the untreated cells. The FACS analysis was done using Cell Quest Software (Becton Dickson, NJ, USA instrument at NCCS, Pune, India).

The efflux of rhodamine 123 in MCF7R cells in the absence or presence of esculetin derivatives was used to assess their P-gp activity as reported. [42] To determine the IC_{50} of the esculetin derivatives, cells were incubated at 37 ℃ with 5 µM rhodamine 123 for 30 min. The control wells were devoid of the test compounds. The cells were washed in phosphate buffered saline and placed at 37 ℃ in the incubator for 10 mins to efflux the Rhodamine 123. The intracellular levels of rhodamine 123 were quantified by spectrofluorimetry using a SpectraMax spectrofluorimeter (Molecular Devices, Sunnyvale, CA, USA) (excitation and emission wavelengths were 485 and 535 nm in 96 well black plates). The percentage of Rhodamine 123 accumulations in control cells not exposed to P-gp inhibitors was arbitrarily set at 100 %. The data obtained was then used to calculate the amount of Rhodamine 123 effluxed out of the cell for graphical representation.

IC_{50} values for inhibition of P-gp activity, which correspond to half-maximal effective concentration (EC_{50}) values for increasing rhodamine 123 efflux were determined using the Prism software (non-linear regressions).

Total protein concentration was measured using Pierce™ BCA kit using Bovine serum albumin as standard. The protein values obtained were used to normalize Rhodoamine 123 with the total protein content in the cell. The P-gp inhibitory potency IC_{50} values for the esculetin derivatives were obtained from the following equation:

$$E = E_o\ (IC_{50}^s / IC_{50}^s + 1)$$

Where, E = efflux in presence of inhibitor; E_o = efflux in absence of inhibitor; I = inhibitor concentration, IC_{50} = concentration that exhibit 50 % inhibition, s= slope factor)

2.2.4. Statistics

Experimental data were routinely expressed as means ± SEM from at least three independent experiments. Statistical analysis of quantitative data was performed with a student's t-test and analysis of variance (ANOVA).

2.3. Computational Methods

2.3.1. Homology Modeling of Human P-Glycoprotein

The three-dimensional structure of human P-gp was not available. Therefore, the homology modeling approach was used to predict the three-dimensional structure of human P-gp, similar to earlier studies. [22, 25, 27, 31, 32, 42] The amino acid (1280 aa) sequence of human P-gp (P08183) was retrieved from the UniProtKB database and the sequence alignment was performed using a basic local alignment search tool (NCBI/BLAST). The murine P-gp showing the highest match with 87 % of sequence identity (4KSB.pdb) was selected as a template to predict the three-dimensional structure of human P-gp by homology modeling using modeler version 9.15 software. [41, 43] The stereochemical quality and validation of the predicted human P-gp model were accessed by Ramachandran plot using PROCHECK program and ProSA web-server, respectively. [44, 45] This P-gp model was used for a molecular docking study to explore the binding mechanism of Esculetin and its derivatives.

2.3.2. Molecular Docking Studies of Esculetin and Its Derivatives Against Human P-gp

The molecular docking approach has been widely used to infer the selectivity profile and the critical interactions between the active site pocket of receptors and the inhibitor molecules. [46, 47] The molecular docking studies of esculetin and its derivatives against the human P-gp were performed using the Autodock 4.2 software. [48] The receptor structure of human P-gp was prepared using Autodock wizard. The molecular structures of esculetin and its derivatives (E-INH, E-HBA, and E-BH) were generated and geometrically optimized by the density functional theory (DFT) method using the B3LYP/6-31G** basis set. [49] The optimization calculations were performed with the help of Guassian'09 software. [50] The P-gp structure was refined by substituting the non-polar hydrogen atoms with the polar hydrogen atoms and by adding the Kollman united atom charges using Autodock wizard. Similarly, gasteiger charges and hydrogen atoms were added to the esculetin and its de-

rivatives. The grid map for the esculetin and its derivatives over the P-gp receptor was calculated by assuming that it would cover the ligand and the active site pocket of the P-gp receptor. The grid size was set to 52 Å ×54 Å ×58 Å for P-gp with 0.375 Å grid spacing. The Lamarckian genetic algorithm with 150 randomly placed entities, 2,70,000 generations, 2,500,000 energy evaluations, and a 1 Å step size for translation was used for the docking process, with a total of 100 runs per compound. The earlier crystallographic and modeling studies showed multiple drugs and substrate binding pockets for P-gp. [42, 44, 46, 50] All these binding pockets contain a few common amino acid residues, which stabilize the substrates/inhibitors and P-gp complexes. Therefore, amino acid residues such as Met69, Pge72, Tyr307, Phe336, Leu339, Phe343, Gln725, Phe728, Phe732, Phe978, and Val982 were chosen as flexible residues during molecular docking studies similar to the earlier report. [42] The favored docked complexes of P-gp and esculetin derivatives having the highest binding affinity with the lowest energies were selected and analyzed for hydrogen bonding and hydrophobic interactions. The Van der Waals, electrostatic, and hydrogen bonding energies for interacting residues from favorable docked complexes of P-gp and esculetin derivatives were also calculated. The pictorial presentation of favorable docked complexes and their molecular interactions was made by Pymol (Molecular Graphics System, Version 1.8 Schrödinger, LLC) and LigPlot software. [51]

2.3.3. Molecular Dynamics Simulation Protocol

The lowest energy stable docked complex of P-gp and E-BH was embedded into the POPC (1-palmitoyl-2-oleoyl-sn-glycero-3-phosphocholine) lipid bilayer using the CHARMM-GUI web server. [52, 53] The coordinates for the lipid bilayer were obtained from the OPM database. [54] The CHARMM36 force-field was used to derive the parameters for lipids and P-gp, while the PRODRG server was used to generate the parameters for the ligand molecule. The MD simulation was performed with the help of GROMACS package version 5.0.7. [55] The equilibration protocol consisted of steepest descent energy minimization followed by 200 ps of MD in NVT ensemble at 300 K and 1 ns of MD in NPT ensemble with position restraints applied to P-gp-lipid bilayer complex. Finally, the system was subjected to a production MD run of 100 ns at 300 K temperature and 1 bar pressure under the isothermal-isobaric (NPT) ensemble. A time step of 2 fs was used throughout the simulation with the periodic boundary conditions. The LINCS algorithm was applied to restrain all bonds to a hydrogen atom and permit a time step of 2 fs. [56] The long-range electrostatic interactions were calculated by employing the PME algorithm with a cutoff distance of 1.2 nm. [57] The simulation trajectories were analyzed using the VMD software. [58] The snapshot structures of P-gp and E-BH simulated complex at different time intervals were selected and analyzed for the hydrogen bonding and hydrophobic interactions using the Ligplot software and the pictorial representation was made by Chimera software. [59]

3. Results and Discussions

3.1. Anti-Proliferative Activity Assay

Figure 1 shows the % cell toxicity using MCF7 and MCF7R cell lines. The MTT assay was done at 24, 48, and 72 h for the different esculetin derivatives. Concentration dependant cell death was observed for Esculetin and the hydrazine derivatives. Almost similar cytotoxic values were obtained for both cell lines.

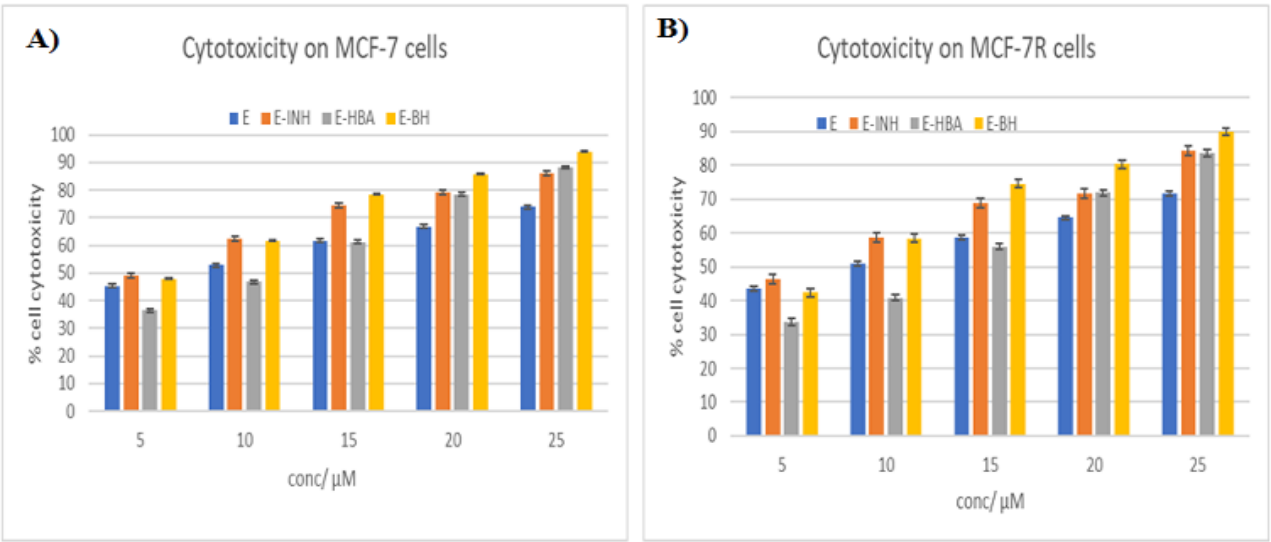

Figure 1. *Cytotoxic effects of esculetin derivatives on A) MCF-7 and B) MCF-7 R cells observed by MTT assay for 72 h. [24 and 48 h data are included in the SI].*

3.2. Rhodamine 123 Accumulation Studies

As compared to the parental MCF7 cells, the accumulation of rhodamine 123 in MCF7R cells was less, depicting P-gp mediated efflux of the dye in the MCF7R cells. While, in the presence of verapamil (50 μM) used as the reference; known to fully inhibit P-gp activity. [60] Rhodamine 123 accumulation in MCF7R cells was restored to the level found in MCF7 cells. In contrast, verapamil does not alter the rhodamine 123 level in MCF 7 cells (Figure 2). When interpreting data from the rhodamine 123 transport assay the dye is partly metabolized to rhodamine 110 through deacetylation followed by its glucuronidation. [61]

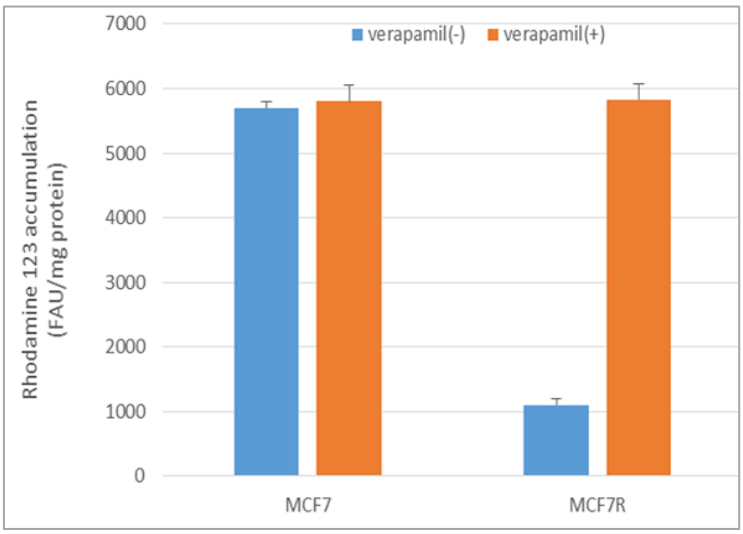

Figure 2. *Accumulation of rhodamine 123 in MCF-7 and MCF7R cells. Cells were exposed to 5 μM rhodamine 123 for 30 min at 37 ℃ in the absence or presence of 50 μM verapamil and quantified by spectrofluorimetry. Data are expressed as fluorescence arbitrary unit (FAU)/mg protein and are the mean ± SEM of three independent experiments.*

Drugs that are known to interfere with the mitochondria usually decrease the mitochondrial membrane potential and increase the cellular accumulation of rhodamine 123 in P-gp expressing cells by inhibiting its efflux. However, the mitochondrial membrane potential studies have not been evaluated for the esculetin derivatives in the current studies. The original sensitive culture contained only non-expressing P-gp cells (Figure 3A). As the cells developed resistance via the stepwise increments of doxorubicin (10 to 600 nM) resulting in resistant MCF-7 sublines, with a high percentage of the cells expressing active P-gp The fraction of cells that had P-gp activity was greater than the P-gp non-expressing cells in number as observed from the histogram exhibiting a single peak of low fluorescence (Figure 3B).

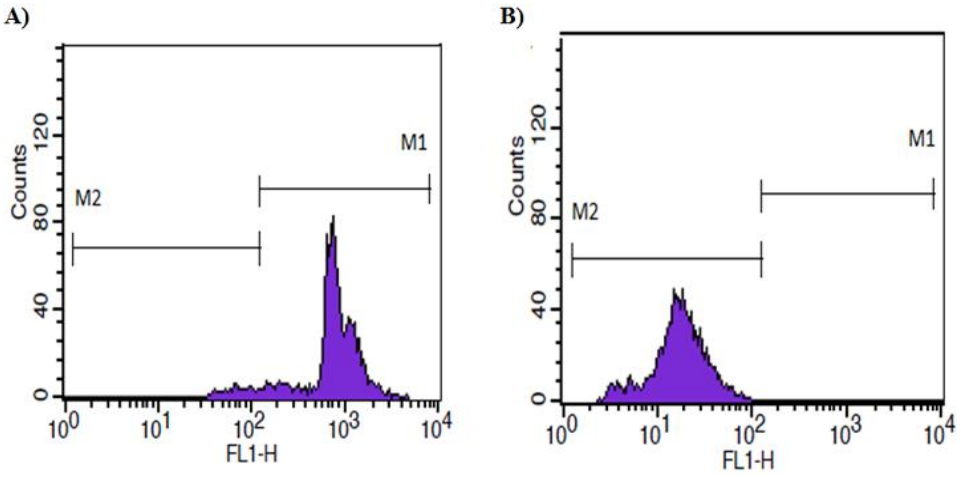

Figure 3. *Flow cytometry histogram of the rhodamine 123 accumulation assay; A) sensitive MCF-7 cell line and B) resistant MCF-7 subline. M1 represents the high fluorescence (FL) region, M2 represents the low FL region.*

3.3. Determination of P-gp IC50 Values for the Esculetin Derivates as P-gp Inhibitors

The concentration-dependent effects of esculetin and hydrazine derivatives on the cellular accumulation of rhodamine 123 were determined in MCF7R cells. To estimate inhibition of P-gp activity for the esculetin derivatives the cellular uptake was evaluated (Figure 4). Firstly, all derivatives were tested at concentrations ranging from 5-25μM in 0.1 % DMSO used as a vehicle. Confocal studies for E-BH at 5μM, exhibited a substantial intrinsic fluorescence signal within the MCF7R cells, while no significant accumulation was detected with the parent compound esculetin (Figure 4A).

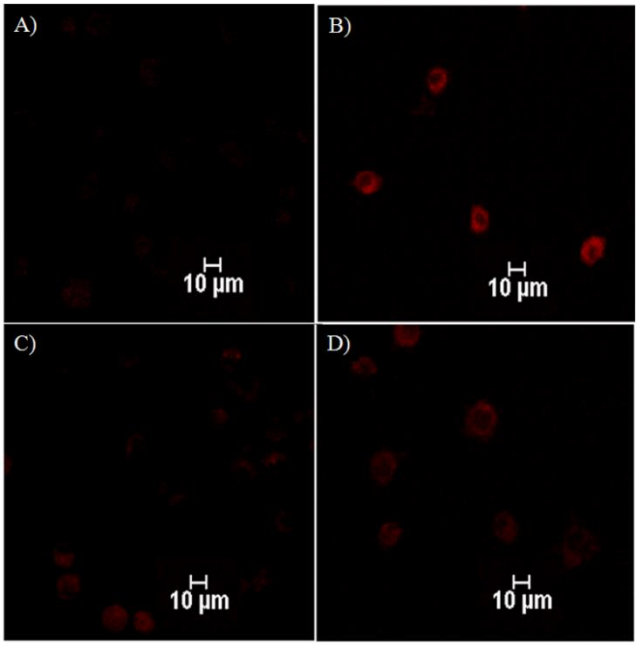

Figure 4. *Fluorescence imaging of esculetin derivatives uptake using TRITC filter; A) Esculetin (E), B) E-BH, C) E-HBA and D) E-INH.*

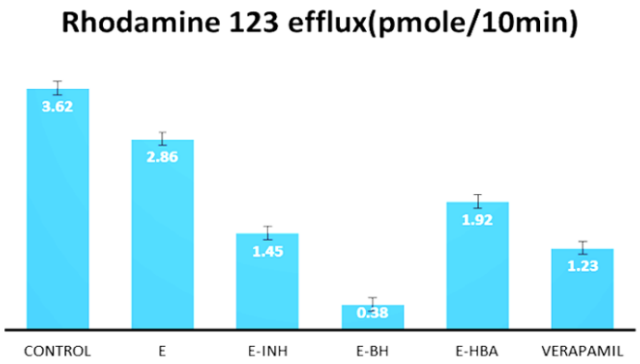

Figure 5. *Efflux of rhodamine 123 in MCF7/R cells. Verapamil 5 μM was used as a positive control.*

The potency of E-BH was then measured in comparison with the positive controls. Verapamil (5 μM) increased R-123 uptake by 3-fold, respectively. [62, 63] Exposure to 5 μM of E-BH induced a higher accumulation of R-123 (9.5 times the control level) as depicted in Figure 5.

The E-BH significantly inhibited rhodamine 123 efflux as compared to other esculetin derivatives. The IC_{50} values for verapamil and esculetin derivatives were calculated using the formula described in Materials and methods and is computed in Table 1.

Table 1. *P-gp inhibitory potential based on rhodamine 123 efflux assay.*

Drug	μM of Esculetin derivatives (IC_{50})
Esculetin	135.5±22.6
E-INH	16.3±1.6
E-BH	8.4±1.83
E-HBA	11.6±2.1
Verapamil	15.1±2.3

3.4. Computational Studies on Human P-gp and Esculetin Derivatives

3.4.1. Homology Modeling of Human P-gp

To corroborate the experimental results and to understand the molecular mechanism of P-gp inhibition by esculetin derivatives, homology modeling, molecular docking, and MD simulation studies were performed. The three-dimensional structure of human P-gp was predicted by a homology modeling study using the murine P-gp as a template structure having an 87% sequence identity (Figure S6). The 50 three-dimensional model structures of P-gp were generated and the best model was selected based on the discrete optimized protein energy (DOPE) score. The 10000 steps of steepest descent energy minimization were performed on the predicted model of P-gp to remove the steric hindrances and ensure structural stability (Figure 6).

Further, the validation is a key step to accessing the quality and reliability of the P-gp model; therefore, the stereochemical analysis of P-gp model using the Procheck server. Ramachandran plot analysis of the human P-gp model showed that 90% of residues are in the most favorable region and 9.3% of residues are in the allowed regions, which confirms the good quality of the predicted model (Figure S7).

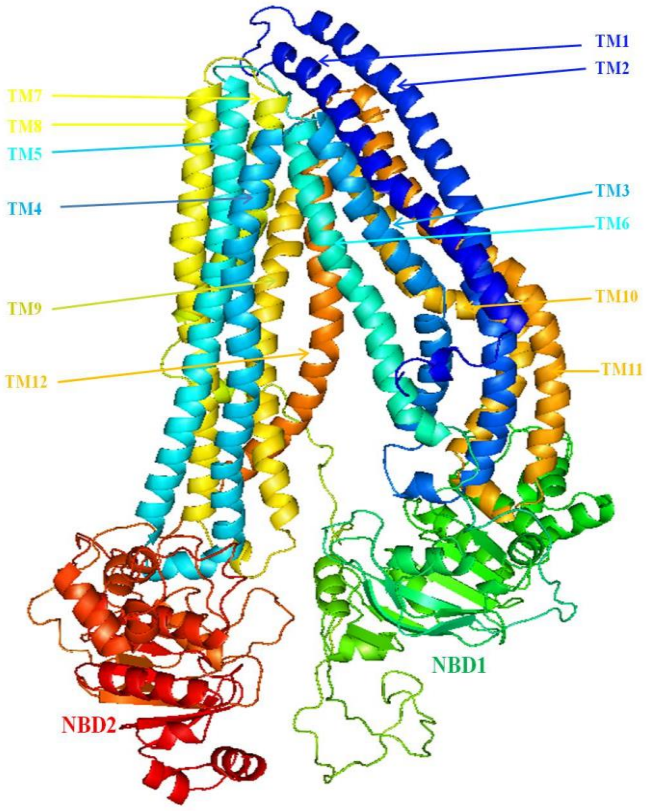

Figure 6. *Predicted three-dimensional structure of human P-gp using homology modeling study.*

Table 2. *Predicted amino acid regions for transmembrane (TMDs) and nucleotide-binding domains (NBDs) from the human P-gp model.*

Amino acid regions	Transmembrane Domains No.	Amino acid regions	Loop/Turns
1-86	Helices/TM1	87-96	Loop
97-164	TM2	165-169	Loop
170-210	TM3	211-212	Loop
213-267	TM4	268-269	Loop
270-322	TM5	323-329	Loop
330-369	TM6	381-626	NBD1/Helices/Sheets/Loops
627-683	Linker Region	684-698	Loop
699-740	TM7	741-746	Loop
747-797	TM8	798-810	Loop
811-852	TM9	853-855	Loop
856-909	TM10	910-912	Loop
913-966	TM11	967-976	Loop
971-1013	TM12	1014-1026	Loops
1027-1280	NBD2		

Furthermore, the overall quality of the P-gp model was predicted by the ProSA server. The Z-score (-12.73) indicates that the P-gp model is in the range of native conformation of proteins, which proves the quality of the model is acceptable.

The inward-facing conformation of P-gp contains two trans-membrane (TMD1 and TMD2) domains which are associated with the other two nucleotide-binding domains (NBD1 and NBD2) (Table 2). Each TMD contains six alpha-helical segments which are linked to NBDs by intracellular loops (ICL), as observed in template murine P-gp. [64] The intracellular helix is forming ball and socket joints in between the TMDs and NBDs segments. The overall structural features of predicted human P-gp are in good agreement with murine P-gp. This P-gp model was used for molecular docking studies with esculetin and its derivatives.

3.4.2. Molecular Docking of Esculetin and Its Derivatives Against the Human P-gp

The molecular docking results of esculetin and its derivatives with human P-gp are depicted in Figure 7 and the supplementary figure S8. The E-BH showed promising anti-P-gp activity in the *in-vitro* study which is substantiated by the lowest energy stable complex produced in the docking experiment. Therefore, herein the detailed docking result of P-gp with E-BH (Figure 7), and the remaining docking results (esculetin and other derivatives) are provided in the supplementary information (Figure S8).

The energetically stable docked complex (-9.02 kcal/mol) of P-gp and E-BH is depicted in Figure 7. In this favorable docked complex, the E-BH binds in deep transport active substrate-binding cavity located at the interface between the transmembrane domain of P-gp by forming strong hydrogen bonding and hydrophobic interactions (Figure 7B, Table 3). The Tyr307 and Gln725 residues were involved in hydrogen bonding interactions with E-BH. The hydroxyl (O4) group of E-BH was involved in bifurcated interactions with phenolic OH of Tyr307 and the amino (NE2) group of Gln725 by maintaining the 2.53 Å and 2.72 Å bond distances, respectively. These hydrogen bonding interactions might be providing the suitable conformational space to E-BH within the catalytic pocket of P-gp to form an energetically stable docked complex. Additionally, the Phe728, Ala729, Phe732, Leu975, Phe978, and Val982 residues from the transmembrane domains of P-gp were involved in hydrophobic contacts with E-BH (Figure 7B). Similar results were reported in earlier docking studies of human P-gp and drug molecules. [25, 42] According to the preceding studies, the hydrophobic residues from the substrate-binding pocket of human P-gp have a crucial role in the smooth transport of drugs/substrates across the membrane. [43] Therefore, the observed hydrogen bonding and hydrophobic interactions might be helpful in the proper positioning of E-BH in the substrate binding pocket to inhibit or block the drugs/substrate efflux mechanism of P-gp.

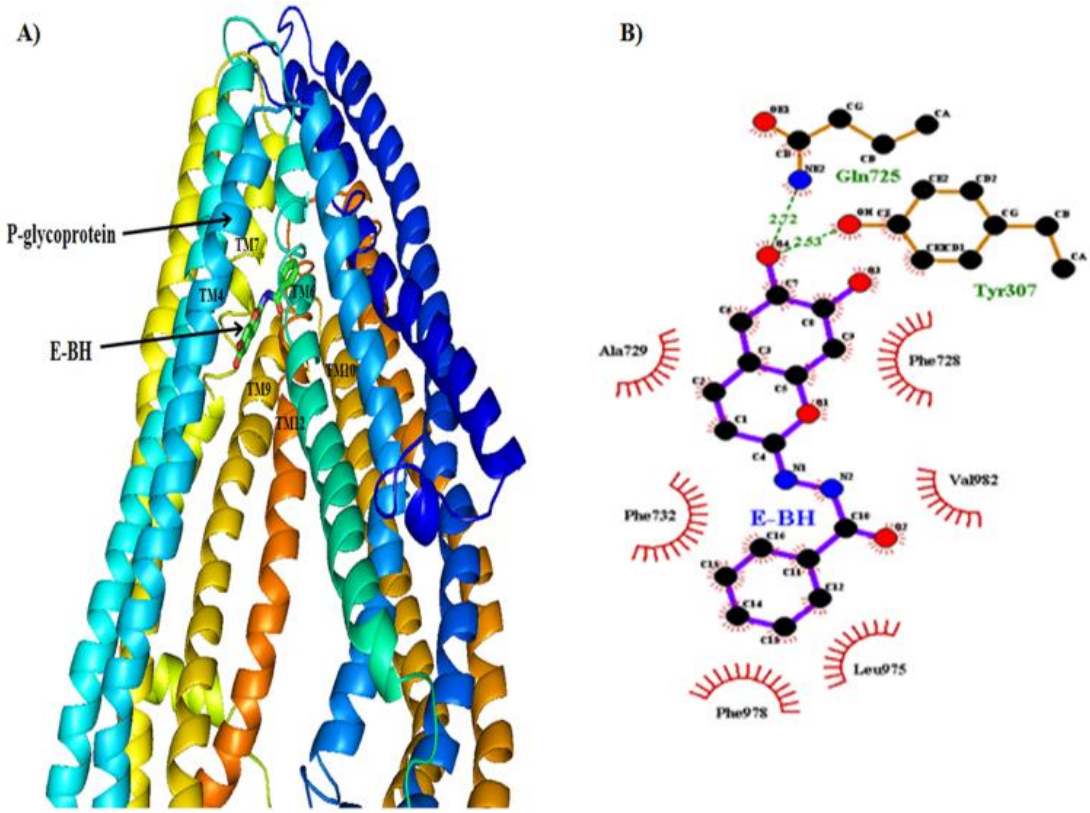

Figure 7. *A) Energetically favorable docked complex of P-gp and E-BH, and B) Hydrogen bonding and hydrophobic interactions from favored docked complex of P-gp and E-BH.*

Table 3. *Intermolecular hydrogen bonding and hydrophobic interactions between the favorable docked complexes of Esculetin and its derivatives with human P-gp.*

Sr. No.	Atoms Involved 1-2-3 in hydrogen bonding	Distance in Å	Binding Energy in kcal/mol	Fig. Ref.
Benzoyl Hydrazide (E-BH) with P-glycoprotein				
1	Tyr307-OH.....O4-E-BH	2.53		
2	Gln725-NE2.....O4-E-BH	2.72	-9.02	7B
3	Phe728, Ala729, Phe732, Leu975, Phe978, Val982	Hydrophobic interactions		
4-Hydrazino Benzoic Acid (E-HBA) with P-glycoprotein				
4	Tyr307-OH.....O3-E-HBA	2.76		
5	Gln725-NE2.....O2-E-HBA	2.59	-8.60	S8-A
6	Phe72, Phe728, Ala729, Phe732, Leu975, Phe978, Ser979, Val982	Hydrophobic interactions		
Isonicotyl Hydrazide (E-INH) with P-glycoprotein				
7	Gln725-NE2.....O3-E-INH	2.67		
8	Gln725-NE2.....O4-E-INH	2.44	-8.11	S8-B
9	Phe72, Phe728, Ala729, Phe732, Ser733, Ile736, Leu975, Phe978, Val982	Hydrophobic interactions		
Esculetin (E) with P-glycoprotein				
10	Tyr307-OH.....O3-Esculetin	2.83		
11	Tyr307-OH.....O4-Esculetin	2.61		
12	Tyr310-OH.....O2-Esculetin	3.15	-6.27	S8-C
	Gln725-NE2.....O3-Esculetin	2.57		
	Phe336, Phe728	Hydrophobic interactions		

Further, the calculated hydrogen bonding, Van der Waals, and electrostatic energies for interacting residues support the docking results (Table S1). Similar docking results were also obtained for the Esculetin and its other derivatives against the P-gp (Figure S8, Table 2, and Table S1). The binding energy pattern of favorable docked complexes of P-gp with E-BH and other esculetin derivatives is in line with experimental observations of P-gp inhibition by E-BH, esculetin, and its derivatives (Table 1). More hydrophobic interactions between esculetin derivatives and catalytic residues from the potential substrate binding site of P-gp produced the lowest energy stable docking complexes (Figures 7 and S8).

3.4.3. MD Simulation Study on a Favorable Docked Complex of E-BH and P-gp

Molecular dynamics simulation was performed to get structural insight into the conformational dynamics of TMDs/NBDs domains and to understand the inhibition mechanism of human P-gp by E-BH. The dynamic stability of the P-gp and E-BH complex was monitored by calculating the root mean square deviation (RMSD) of Cα atoms of the protein backbone throughout the 100 ns of simulation and shown in Figure 8A. The RMSD displayed a rapid increase in the first 30 ns, followed by a plateau over the simulation time. The RMSD value ranged from 7.5 nm to 8.5 nm throughout the simulation. The large deviation in RMSD may be due to the 'breathing motions' of the protein as described earlier by using MD alongside double electron-electron resonance spectroscopy. [29] The RMS fluctuation analysis showed the highest degree of fluctuations in residues (Cα atoms) from the NBD domains, the extracellular loop connecting TMD domains, and the terminal regions (Figure 8B). Further, the displacements (RMSD) of individual helices from the TMDs and NBDs showed the highest degree of fluctuations for TM1, TM2, TM7, TM8, and NBD1 during the simulation (Figure 8C-8E). This may accentuate the flexible nature of the P-gp transporter. The TM4, TM6, TM10, and TM12 showed good stability in simulation which provides the steady interface of hydrophobic residues for interactions with E-BH and is comparable with the previous experimental and computa-

tional observations (Figure 8C-8E). [8, 25, 64, 65]

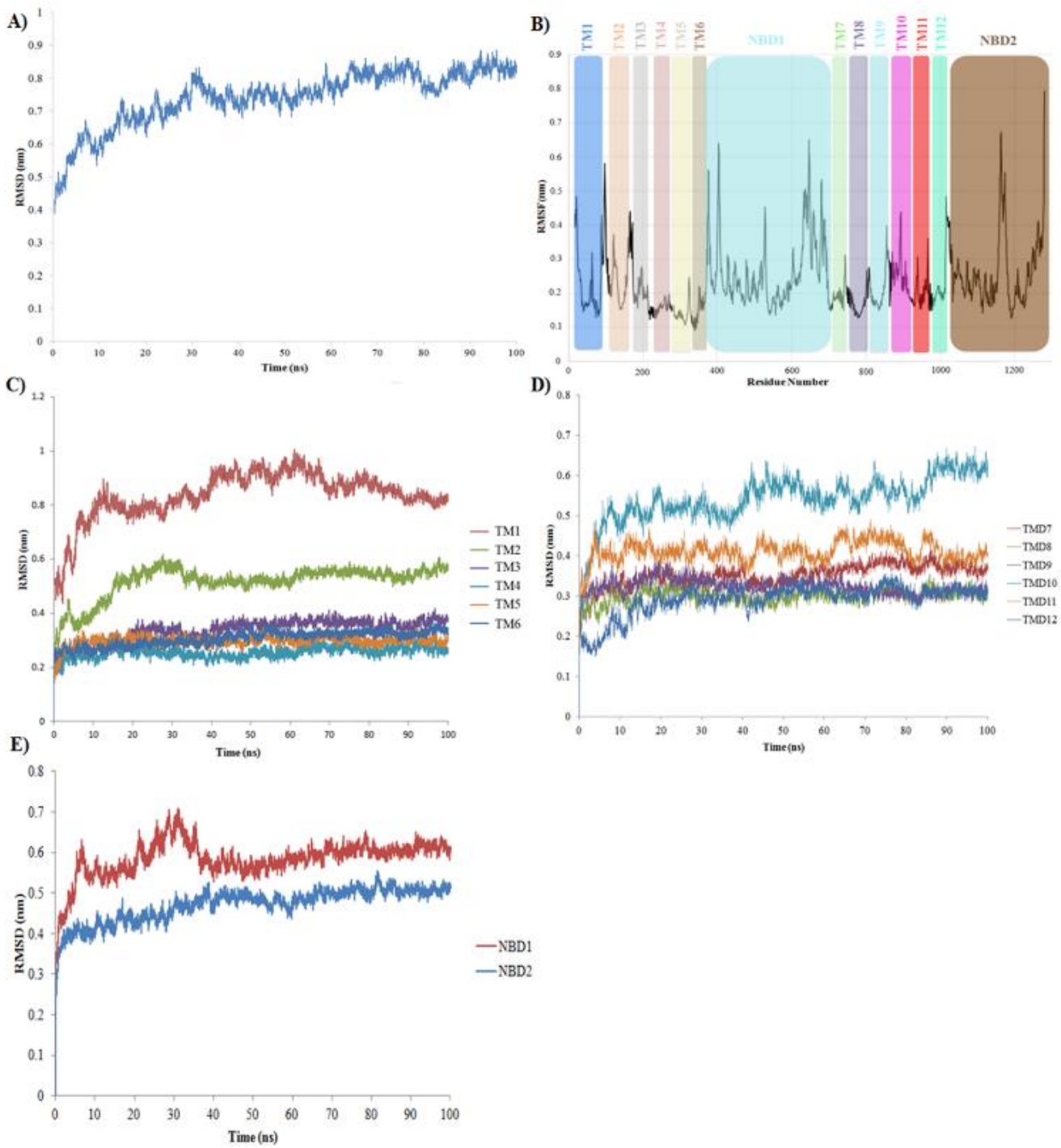

Figure 8. *A) RMSD fluctuation of P-gp and E-BH complex during 100 ns of MD simulation study. B) RMSF fluctuations for 1280 residues of human P-gp during 100 ns of simulation, C) RMSD fluctuations in TM helices of TMD1, D) RMSD fluctuations in TM helices of TMD2 and E) RMSD fluctuations in NBD1 and NBD2 of human P-gp.*

Furthermore, the quantitative investigations of movements of TM helices have been made by calculating the distances between the top and bottom residues of adjacent TMs helices of two TMDs that are facing each other during the simulation (Figure 9).

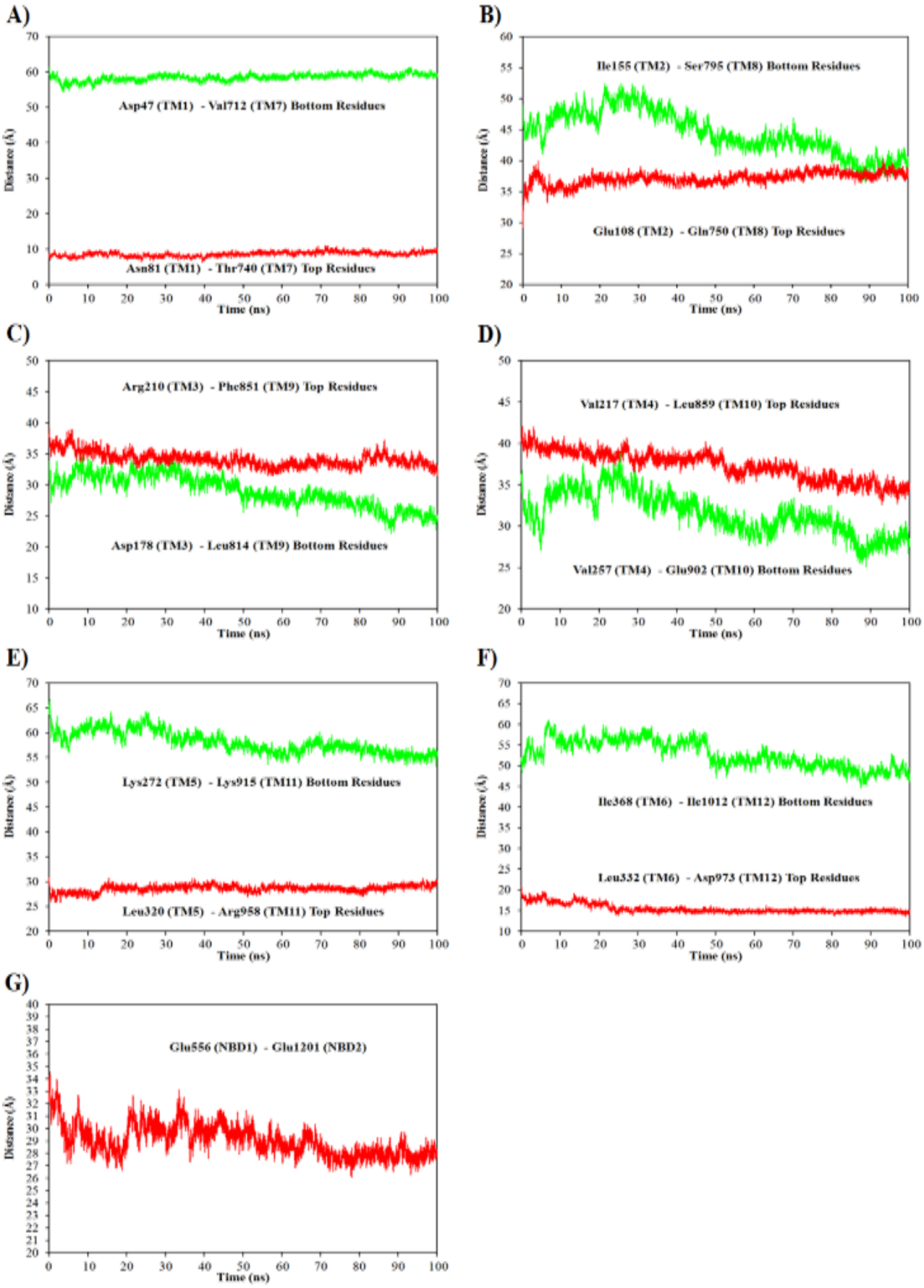

Figure 9. *Calculated the distances between the top and bottom residues of adjacent TMs helices facing each other in two TMDs during simulation; A) Distance between the top (red color) and bottom residues (green color) from TM1 and TM7 helices, B) TM2 and TM8, C) TM3 and TM9, D) TM4 and TM10, E) TM5 and TM11, D) TM6 and TM12 and G) Distance between NBD1 and NBD2 domains.*

The smooth movement of TM1 and TM7 helices was observed during the simulation (Figure 9A). A very small and steady movement in top residues of TM2-TM8 and TM5-TM11 was observed; while the bottom residues of helices come closer (Figures 9B and 9E). This leads to slightly opening the conformational space of P-gp in an outward direction during the simulation. In addition, the top and bottom residues of TM3-TM9 helices showed a decrease in distances which indicated that TM3 moved along with TM9 in the same direction (Figure 9C). A similar trend was observed for TM4-TM10 and TM6-TM12 helices (Figures 9D and 9F). Also, the distances between the NBD1 and NBD residues were decreased within the range of 4 Å to 6 Å throughout the simulation time (Figure 9G). These results indicate that a small movement of TMDs and NBDs domains of P-gp was observed in the simulation. The overall conformational stability of the P-gp during simulation is due to the stable molecular interactions between the P-gp and E-BH.

Moreover, the MD simulation results were also analyzed by selecting the snapshot structures at various time intervals and subjected to molecular interactions analysis between P-gp and E-BH complex (Figures 10 and S9, Table S2). At 100 ns (Figure 10), the E-BH forms hydrophobic interactions with Ala729, Phe732, Phe978, and Val982 residues from the catalytic pocket of P-gp, similarly as observed in the docking results (Figure 7B and Table 3). Also, the Met69, Tyr310, Thr333, Phe336, Phe728, Phe732, Leu975, Phe978, Ser979, Val982, and Phe983 residues of P-gp were involved in hydrophobic interactions with E-BH throughout the simulation (Figure S9 and Table S2).

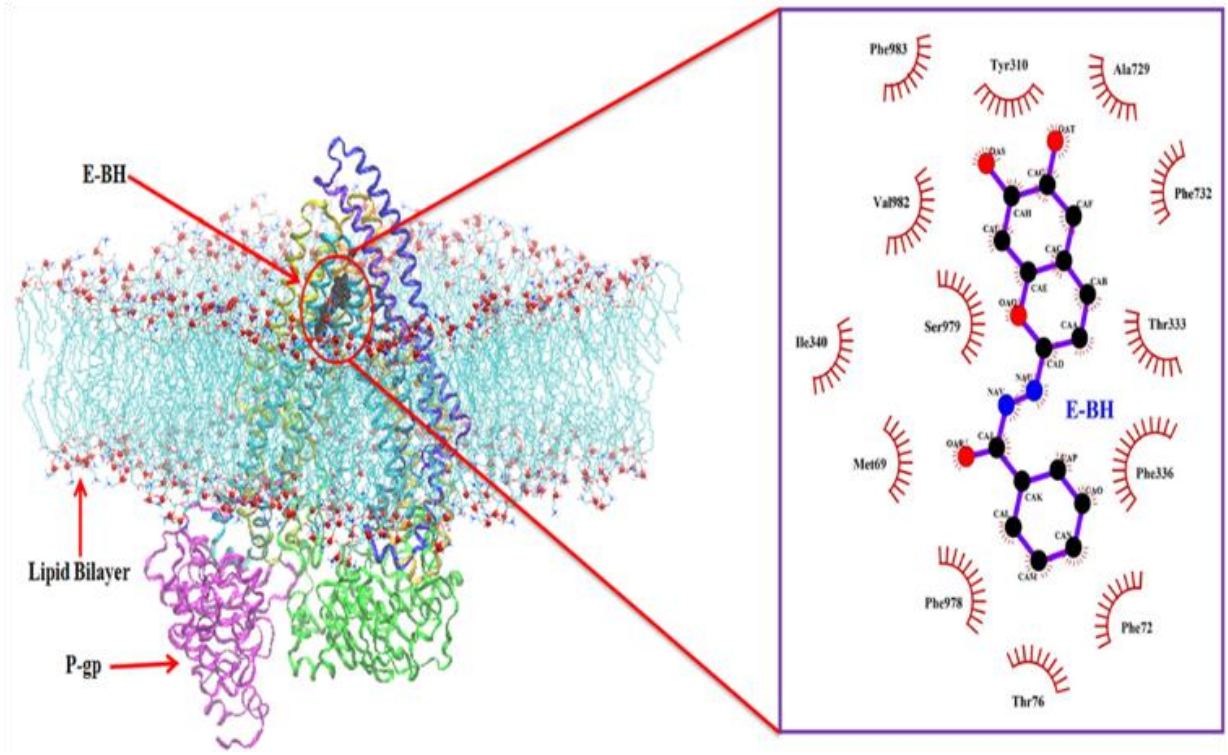

Figure 10. *Depicted molecular interactions between E-BH and P-gp after 100 ns of MD simulation study.*

Remarkably, the Phe72 (TM1), Ty310 and Phe336 (TM6), Phe728 and Phe732 (TM7), Phe978 and Phe983 (TM12) residues are involved in the inhibition of P-gp activity and were noticed consistently during the simulation period (Figure 11 and Table S2). Similar interactions were noticed in the earlier molecular docking and MD simulation studies of P-gp with inhibitor molecules. [25, 65, 44, 66-72] This again confirms the acceptable quality of the predicted model of human P-gp. Additionally, the E-BH showed a tendency to preserve the stable binding interactions with P-gp throughout the simulation period. From these results, it is anticipated that fluctuations of TMD and NBD domains during the simulation did not affect the molecular interactions between the E-BH and catalytic residues of P-gp.

In addition to this, the TM1 and TM7 domains were interacting with each other in such a way that it would block the exit side or the efflux motion path of the P-gp transporter (Figure 12). The interactions of E-BH to the P-gp substrate binding site may render the fully open or outward conformation of P-gp during the simulation. Thus, considering all these noticed facts, the E-BH might be acting as a good anticancer agent in chemotherapeutic treatment by inhibiting the drug efflux mechanism of the P-gp transporter across the membrane. Therefore, the performed molecular docking and

MD simulation studies may pave the way to get a structural insight into conformational dynamics of P-gp and E-BH mediated inhibition of P-gp.

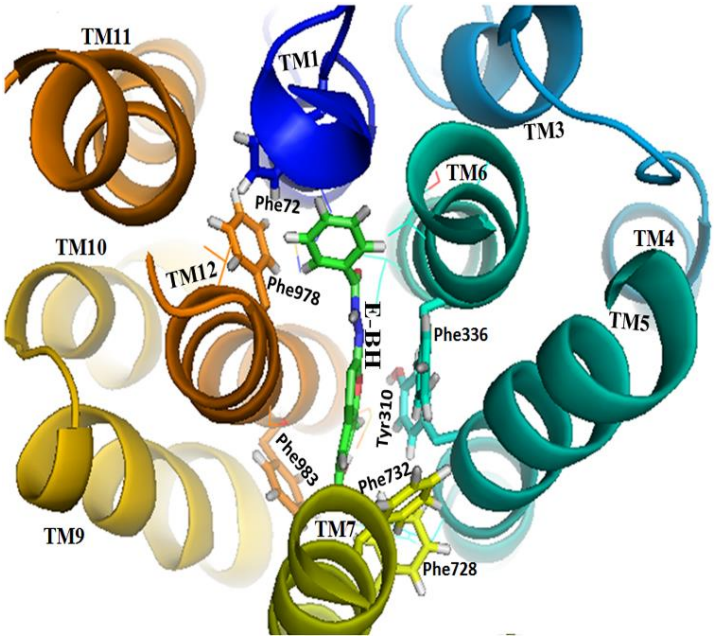

Figure 11. *The top view of the human P-gp and E-BH simulated complex showed the interactions from the hydrophobic residues with the E-BH during simulation.*

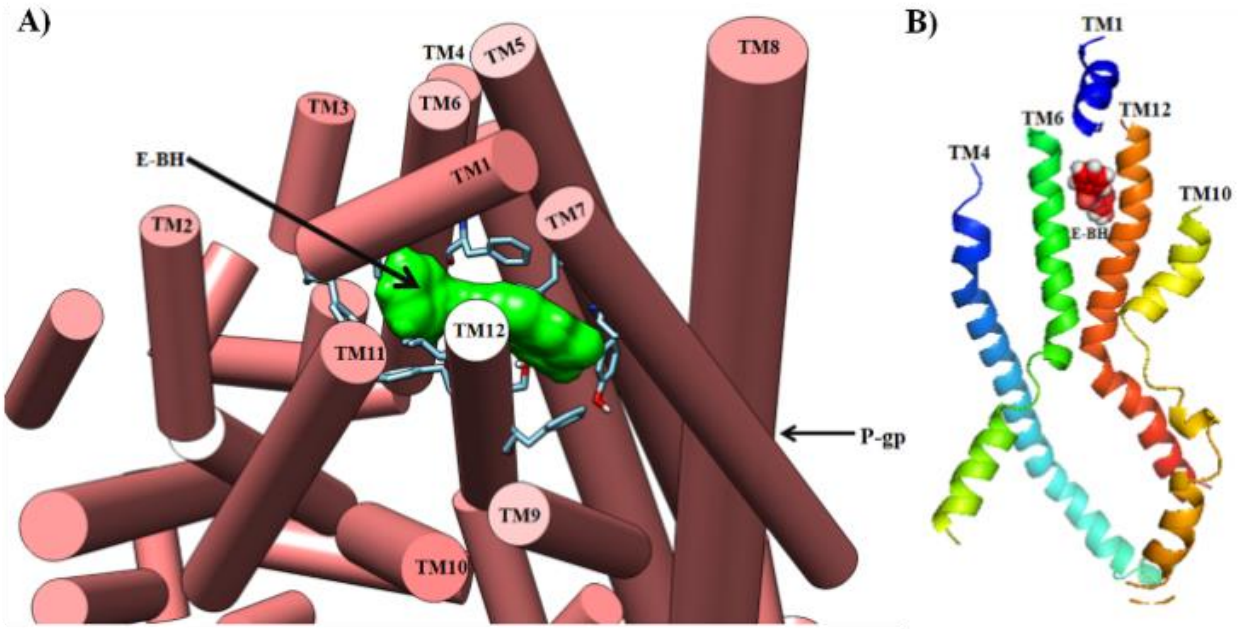

Figure 12. *A) Depicted the role of TM1 and TM7 domains in preventing the exit of E-BH from the human P-gp transporter by blocking the exit site. B) The location of E-BH in the interface between transmembrane TM4, TM6, TM10, and TM12 domains and the TM1 domains was blocking the exit site of the P-gp transporter.*

Moreover, the docking and MD simulation results anticipated that aromatics and hydrophobic residues (Met69, Tyr310, Thr333, Phe336, Phe728, Ala729, Phe732, Leu975, Phe978, Ser979, Val982, and Phe983) of P-gp are forming strong hydrophobic contacts with E-BH (Figures 7 and 10) and Esculetin, E-INH, E-HBA (Figures S8 and S9, Table 3). This data suggested that the activity of P-gp is most probably controlled by hydrophobic interactions and less by hydrogen

bonding and other interactions. Hence, the H-bonds observed in docking studies could be involved in the formation of tight binding of E-BH within the catalytic pocket to inhibit the activity of P-gp. These results are in line with the earlier mutational studies of human P-gp. [2] Further, the analysis of murine-P-gp crystal complexes showed that all the above-mutated residues were involved in hydrophobic contacts with peptide inhibitor molecules, except the Gln725, which is involved in H-bond with the carbonyl oxygen of cyclic hexapeptide inhibitors. [73] Moreover, based on the involvement of hydrophobic residues in the drug efflux mechanism, the P-gp was termed as "hydrophobic vacuum cleaner". [74] All the obtained docking and simulation results are comparable with the earlier experimental and computation studies. Therefore, the predicted conformational dynamics of P-gp and the molecular interactions mediated inhibition of P-gp efflux transporter may pave the way to design the potent and selective inhibitors of P-gp for the treatment of cancer, Alzheimer's, Parkinson's, and Epilepsy.

4. Conclusions

The natural coumarin hydrazine derivatives were successfully synthesized and characterized by various spectroscopic techniques. The E-BH has shown potent P-gp inhibitory activity (8.0 μM) in rhodamine 123 accumulation assay as compared to other esculetin derivatives (E-INH and E-HBA). These results were substantiated using a molecular docking study. The E-BH was forming an energetically (-9.02 kcal/mol) stable complex with P-gp by forming hydrogen bonding and hydrophobic interactions. Similar interactions were found in earlier crystallographic and computational studies and validated by performing molecular dynamics simulations. Docking and MD simulation results anticipated that aromatics and hydrophobic residues such as Met69, Tyr310, Thr333, Phe336, Phe728, Ala729, Phe732, Leu975, Phe978, Ser979, Val982, and Phe983 were forming strong hydrophobic contacts with E-BH and other Esculetin derivatives. This confirms that the activity of P-gp is most probably controlled by hydrophobic interactions and less by hydrogen bonding and other interactions. Therefore, performed biological experiments and computational predictions may pave the way to design potent and selective P-gp inhibitors or blockers to treat various types of human cancers and other diseases.

Abbreviations

E	Esculetin
E-BH	Esculetin Benzoyl Hydrazine
E-INH	Esculetin Isonicotinyl Hydrazine
E-HBA	Esculeting Hydrazine Benzoic Acid
P-gp	P-glycoprotein
MCF-7/R	MCF-7/Resistant Cell Lines Expressing P-gp
MDR	Multidrug Resistance
MDCK	Madin Darby Canine Kidney Cells
FTIR	Fourier Transform Infrared Spectroscopy
NMR	Nuclear Magnetic Resonance
ANOVA	Analysis of Variance
NCCS	National Centre for Cell Sciences
DFT	Density Functional Theory
LINCS	Linear Constraint Solver for Molecular Simulations
VMD	Visual Molecular Dynamics
MTT	3-(4,5-dimethylthiazol-2-yl)-2,5-diphenyltetrazolium bromide
DOPE	Discrete Optimized Protein Energy

Supplementary Material

The supplementary material can be accessed at https://doi.org/10.11648/j.ajbls.20241203.11

Acknowledgments

Ayesha Khan sincerely acknowledges the Institute of Bioinformatics and Biotechnology for using instrumentation facilities. Mr. Jehangir Sayyed is thanked for technical support.

Author Contributions

Navanath Kumbhar: Formal Analysis

Neelofar Khan: Chemical synthesis and characterization, Wet lab analysis

Ayesha Khan: Conceptualization, Wet lab analysis

Rohit Bavi: Data curation, computational studies

Sagar Barage: Data curation, computational studies

Funding

Ayesha Khan acknowledges the BRNS research grant (2010/37C/55/BRNS2536). Navanath Kumbhar sincerely acknowledges Savitribai Phule Pune University (SPPU) (Formerly Pune University), Pune for providing the SPPU post-doctoral fellowship (ST/BL/2018-2018/0006). Ayesha Khan sincerely acknowledges the Institute of Bioinformatics and Biotechnology for using instrumentation facilities.

Data Availability Statement

The data supporting the outcome of this research work has been reported in this manuscript.

Conflicts of Interest

The authors declare no conflicts of interest.

References

[1] M. M. Gottesman, C. A. Hrycyna, P. V. Schoenlein, U. A. Germann, I Pastan, Genetic analysis of the multidrug transporter, Annu. Rev. Genet. 29 (1995) 607-649. https://doi.org/10.1146/annurev.ge.29.120195.003135

[2] T. W. Loo, D. M. Clarke, Identification of residues in the drug-binding site of human P- glycoprotein using a thiol-reactive substrate, J. Biol. Chem. 272 (1997) 31945-31948. https://doi.org/10.1074/jbc.272.51.31945

[3] S. V. Ambudkar, G Kimchi-Sarfaty, Z. E. Suana, M. M. Gottesman, P-glycoprotein: from genomics to mechanism, Oncogene 22 (2003) 7468-7485. https://doi.org/10.1038/sj.onc.1206948

[4] P. D. Eckford, F. J. Sharom, ABC efflux pump-based resistance to chemotherapy drugs. Chem. Rev. 109 (2009) 2989-3011. https://doi.org/10.1021/cr9000226

[5] B Marquez, B. F. Van, ABC multidrug transporter: Target for modulation of drug pharmacokinetics and drug-drug interactions. Curr. drug targets 12 (2011) 600-620. https://doi.org/10.2174/138945011795378504

[6] S Kunjachan, B Rychlik, G Storm, F Kiessling, T. Lammers, Multidrug resistance: Physiological principles and nanomedical solutions, Adv. Drug Deliv. Rev. 65 (2013) 1852-1865. https://doi.org/10.1016/j.addr.2013.09.018

[7] M. Leopoldo, P. Nardulli, M. Contino, F. Leonetti, G. Luurtsema, N. A. Colabufo. An updated patent revire on P-glycoprotein inhibitors, Expert Opin. Ther. Pat. 29 (2019) 455-461. https://doi.org/10.1080/13543776.2019.1618273

[8] J. Marcoux, S. C. Wang, A. Ploitis, et al., Mass spectrometry reveals synergetic effects to nucleotides, lipids, and drug binding to a multidrug resistance efflux pump, Proc. Natl. Acad. Sci. U. S. A. 110 (2013) 9704-9709. https://doi.org/10.1073/pnas.1303888110

[9] D. Waghray, Q. Zhang, Inhibit or Evade Multidrug Resistance P-Glycoprotein in Cancer Treatment, J. Med. Chem. 61(2018) 5108-5121. https://doi.org/10.1021/acs.jmedchem.7b01457

[10] E. N. Yakusheva, D. S. Titov, Structure and Function of Multidrug Resistance Protein-1 Biochemistry (Mosc) 83(2018) 907-929. https://doi.org/10.1134/s0006297918080047

[11] S. Mollazadeh, A. Sahebkar, F. Hadizadeh, J. Behravan, S. Arabzadeh, Structural and functional aspects of P-glycoprotein and its inhibitors, Life Sci. 214 (2018) 118-123. https://doi.org/10.1016/j.lfs.2018.10.048

[12] K. P. Sigdel, L. A. Wilt, B. P. Marsh, A. G. Roberts, G. M. King, The conformation and dynamics of P-glycoprotein in a lipid bilayer investigated by atomic force microscopy, Biochem. Pharmacol. 156 (2018) 302-311. https://doi.org/10.1016%2Fj.bcp.2018.08.017

[13] Sajid, N. Raju, S. Lusvarghi, S. Vahedi, R. E. Swenson, S. V. Ambudkar, Synthesis and characterization of Bodpy-FL-cyclosporin A as a substrate for multidrug resistance-linked P-glycoprotein (ABCB1), Drug Metab. Dispos. 47(2019) 1013-1023. https://doi.org/10.1124/dmd.119.087734

[14] W. Guo, W. Dong, M. Li, Y. Shen, Mitochondria P-glycoprotein confers paclitaxel resistance on ovarian cancer cells, Onco. Targets Ther. 12 (2019) 3881-3891. https://doi.org/10.2147%2FOTT.S193433

[15] F. Montanari, G. F. Ecker, Prediction of drug-ABC-transporter interaction - Recent advances and future challenges, Adv. Drug Deliv. Rev. 86 (2015) 17-26. https://doi.org/10.1016/j.addr.2015.03.001

[16] J. W. McCormick, P. D. Vogel, J. G. Wise, Multiple drug transport through Human P-Glycoprotein, Biochemistry 54 (2015) 4374-4390. https://doi.org/10.1021/acs.biochem.5b00018

[17] J. Bender, J. Fang, R. Simon, A computational study of the inhibition mechanisms of P-glycoprotein mediated paclitaxel efflux by kinase inhibitors, BMC Syst. Biol. 11 (2017) 1-10. https://doi.org/10.1186/s12918-017-0498-x

[18] J. Wang, N. Seebacher, H. Shi, Q. Kan, Z. Duan, Novel strategies to prevent the development of multidrug resistance (MDR) in cancer, Oncotarget 8 (2017) 84559-84571. https://doi.org/10.18632%2Foncotarget.19187

[19] S. Varghese, A. Palaniappan, Computational Pharmacogenetics of P-Glycoprotein Mediated Antiepileptic Drug Resistance. Open Bioinforma J. 11 (2018) 197- 207. https://dx.doi.org/10.2174/1875036201811010197

[20] L. Domicevica, H. Koldso, P. C. Biggin, Multiscale molecular dynamics simulations of lipid interactions with P-glycoprotein in a complex membrane, J. Mol. Graph. Model. 80 (2018) 147-156. https://doi.org/10.1016/j.jmgm.2017.12.022

[21] E. Barreto-Ojeda, V. Corradi, R-X. Gu, D. P. Tieleman, Coarse-grained molecular dynamics simulations reveal lipid access pathways in P-glycoprotein, J. Gen. Physiol. 150 (2018) 417-429. https://doi.org/10.1085%2Fjgp.201711907

[22] L. Wang, L. Zhang, F. Liu, Y. Sun, Molecular energetics of Doxorubicin pumping by human P-glycoprotein, J. Chem. Inf. Model. 59 (2019) 3889-3898. https://doi.org/10.1021/acs.jcim.9b00429

[23] Z. Bikadi, I. Hazal, D. Malik, K. Jemnitz, Z. Veres, P. Hari, Z. Ni, T. W. Loo, D. M. Clarke, E. Hazai, Q. Mao, Predicting P-glycoprotein-mediated drug transport based on support vector macnine and three dimensional crystal structure of P-glycoprotein, Plos One 6 (2011) e25815. https://doi.org/10.1371%2Fjournal.pone.0025815

[24] L. Chen, Y. Li, H. Yu, L. Zhang, T. Hou, Computational models for predicting substrates or inhibitors of P-glycoprotein, Drug Discov. Today 17(2012) 343-51. https://doi.org/10.1016/j.drudis.2011.11.003

[25] R. Prajapati, A. T. Sangamwar, Translocation mechanism of P-glycoprotein and conformational changes occurring at drug-binding site: Insights from multi-targeted molecular dynamics, Biochim. Biophys. Acta Biomembr. 1838 (2014) 2882-2898. https://doi.org/10.1016/j.bbamem.2014.07.018

[26] M. L. Gonzalez, D. M. A. Vera, J. Laiolo, M. B. Joray, M. Maccioni, S. M. Palacios, G. M. Molina, P. A. Lanza, S. Gancedo, V. Rumjanek, M. C. Carpinella, Mechanism underlying the reversal of drug resistance in P-Glycoprotein-expressing leukemia cells by pinoresinol and the study of a derivative, Front. Pharmacol. 25 (2017) 205. https://doi.org/10.3389/fphar.2017.00205

[27] Cui, C. Y. Cai, H. L. Gao, L. Ren, N. Ji, P. Gupta, Y. Yang, S. Shukla, S. V. Ambudkar, D. H. Yang, Z. S. Chen Glesatinib, a c-MET/SMO Dual Inhibitor, Antagonizes P-glycoprotein mediated multidrug resistance in cancer cells, Front. Oncol. 25 (2019) 313. https://doi.org/10.3389%2Ffonc.2019.00313

[28] J. G. Wise, Catalytic transitions in the human MDR1 P-glycoprotein drug binding sites, Biochemistry 51 (2012) 5125-5141. https://doi.org/10.1021/bi300299z

[29] P. C. Wen, B. Verhalen, S. Wilkens, H. S. Nchaourab, E. Tajkhorshid, On the origine large flexibility of P-glycoprotein in the inward facing state, J. Biol. Chem. 288 (2013) 19211-19220. https://doi.org/10.1074%2Fjbc.M113.450114

[30] J. P. Becker, G. Depret, F. VanBambeke, P. M. Tulkens, M. Prevost, Molecular models of human P-glycoprotein in two different catalytic states, BMC Struct. Biol. 9 (2009) 3.31. J. R. https://doi.org/10.1186%2F1472-6807-9-3

[31] Daddam, M. R. Dowlathabad, S. Panthangi, P. Jasti, Molecular docking and P-glycoprotein inhibitory activity of flavonoids, Interdiscip Sci. 6(2014) 167-175. L. https://doi.org/10.1007/s12539-012-0197-7

[32] Domicevica, P. C. Biggin, Homology modelling of human P-glycoprotein, Biochem. Soc. Trans. 43 (2015) 952-958. https://doi.org/10.1042/bst20150125

[33] A. Tripathi, K. Misra, Inhibition of P-Glycoprotein Mediated Efflux of Paclitaxel by Coumarin Derivatives in Cancer Stem Cells: An In Silico Approach, Comb Chem High Throughput Screen. 19(2016) 497-506. https://doi.org/10.2174/1386207319666160517115158

[34] K. Wang, Y. Zhang, S. I. N. Ekunwe, et al., Antioxidant activity and inhibition effect on the growth of human colon carcinoma (HT-29) cells of esculetin from Cortex Fraxini, Med Chem Res. 20 (2011) 968–974. https://dx.doi.org/10.1007/s00044-010-9426-y

[35] Y. J. Jeon, J. Y. Jang, J. H. Shim, P. K. Myung, J. I. Chae, Esculetin, a Coumarin Derivative, Exhibits Anti-proliferative and Pro-apoptotic Activity in G361 Human Malignant Melanoma, J Cancer Prev. 20 (2015) 106-12. https://doi.org/10.15430%2FJCP.2015.20.2.106

[36] C. Barthomeuf, J. Grassi, M. Demeule, C. Fournier, D. Boivin, R. Bđiveau, Inhibition of P-glycoprotein transport function and reversion of MDR1 multidrug resistance by cnidiadin, Cancer Chemother. Pharmacol. 56 (2005) 173-81. https://doi.org/10.1007/s00280-004-0914-y

[37] V. Kumar, Hydrazone: A promising pharmacophore in medicinal chemistry, J. Pharmacogn Phytochem. 7(2018) 40-43.

[38] N. Duangdee, W. Mahavorasirikul, S. Prateeptongkum, Design synthesis and anti-proliferative activity of some new coumarin substituted hydrazide-hydrazone derivatives, J Chem Sci. 132 (2020) 66. https://doi.org/10.1007/s12039-020-01767-4

[39] H. Morjani, N. Aouali, R. Belhoussine, R. J. Veldman, T. Levade, M. Manfait, Elevation of glucosylceramide in multidrug-resistant cancer cells and accumulation in cytoplasmic droplets, Int. J. Cancer 94 (2001) 157-165. https://doi.org/10.1002/ijc.1449

[40] G. Batist, A. Tulpule, B. K. Sinha, A. G. Katki, C. E. Myers, K. H. Cowan Overexpression of a novel anionic glutathione transferase in multidrug-resistant human breast cancer cells, J. Biol. Chem. 261 (1986) 15544-15549. https://doi.org/10.1016/S0021-9258(18)66748-1

[41] T. L. Riss, R. A. Moravec, A. L. Niles, et al., Cell Viability Assays. In: Sittampalam GS, Grossman A, Brimacombe K, et al., editors. Assay Guidance Manual [Internet]. Bethesda (MD): Eli Lilly & Company and the National Center for Advancing Translational Sciences, 2016. https://www.ncbi.nlm.nih.gov/books/

[42] V. M. Le, E. Jouan, B. Stieger, V. Lecureur, O. Fardel, Regulation of human hepatic drug transporter activity and expression by diesel exhaust particle extract, Plos One 10 (2015) e0121232. https://doi.org/10.1371/journal.pone.0121232

[43] B. Webb, A. Sali, Comparative Protein Structure Modeling Using MODELLER, Curr. Protoc. Bioinformatics 54 (2016) 5.6.1-5.6.37. https://doi.org/10.1002/cpbi.3

[44] R. A. Laskowski, M. W. MacArthur, D. S. Moss, J. M. Thornton, PROCHECK a program to check the stereochemical quality of protein structures, J. Appl. Crystallography 26 (1993) 283-291. https://doi.org/10.1107/S0021889892009944

[45] M. Wiederstein, M. J. Sippl, ProSA-web: interactive web service for the recognition of errors in three-dimensional structures of proteins, Nucleic Acids Res. 35 (2007) W407-W410. https://doi.org/10.1093/nar/gkm290

[46] N. M. Kumbhar, S. K. Nimal, S. Barale, S, Ka.mble, R. S. Bavi, K. D. Sonawane, R. N. Gacche. Identification of novel leads as potent inhibitors of HDAC3 using ligand-based pharmacophore modeling and MD simulation, Scientific Reports, 2022, 12(1): 1712. https://doi.org/10.1038/s41598-022-05698-7

[47] K. S. Gavale, S. R. Chavan, N. M. Kumbhar, S. Kawade, P. Doshi, A. Khan, D. D. Dhavale, α-Geminal disubstituted pyrrolidine iminosugars and their C-4-fluoro analogues: Synthesis, glycosidase inhibition and molecular docking studies, Bioorg. Med. Chem. 25 (2017) 5148-5159. https://doi.org/10.1016/j.bmc.2017.07.026

[48] G. M. Morris, R. Huey, W. Lindstrom, M. F. Sanner, R. K. Belew, D. S. Goodsell, A. J. Olson, Autodock4 and AutoDockTools4: automated docking with selective receptor flexibility, J. Comput. Chem. 16 (2009) 2785-2791. https://doi.org/10.1002%2Fjcc.21256

[49] A. D. Becke, Density functional thermochemistry. III. The role of exact exchange, J. Chem. Phys. 98 (1992). 5648-5652. https://doi.org/10.1063/1.464913

[50] M. J. Frisch, G. W. Trucks, H. B. Schlegel, et al., Gaussian, Inc., Wallingford CT, 2009. https://doi.org/10.4236/jemaa.2016.810020

[51] A. C. Wallace, R. A. Laskowski, Thornton JM LIGPLOT: a program to generate schematic diagrams of protein-ligand interactions, Protein Eng. 8 (1996) 127-134. https://doi.org/10.1093/protein/8.2.127

[52] S. Jo, T. Kim, V. G. Iyer, W. Im, CHARMM-GUI: a web-based graphical user interface for CHARMM, J. Comput. Chem. 29 (2008) 1859-65. https://doi.org/10.1002/jcc.20945

[53] J. Lee, X. Cheng, J. M. Swails, M. S. Yeom, P. K. Eastman, J. A. Lemkul, S. Wei, J. Buckner, J. C. Jeong, Y. Qi, S. Jo, V. S. Pande, D. A. Case, C. L. Brooks, A. D. MacKerell, J. B. Klauda, W. Im, CHARMMGUI Input Generator for NAMD, GROMACS, AMBER, OpenMM, and CHARMM/ OpenMM Simulations Using the CHARMM36 Additive Force Field, J. Chem. Theory Comput. 12 (2016) 405-13. https://doi.org/10.1021/acs.jctc.5b00935

[54] Lomize MA, Pogozheva ID, Joo H, Mosberg HI, Lomize AL, OPM database and PPM web server: resources for positioning of proteins in membranes. Nucleic Acids Res. 2012; 40: D370-D376. https://doi.org/10.1093/nar/gkr703

[55] M. J. Abraham, T. Murtola, R. Schulz, S. Pall, J. C. Smith, B. Hess, E. Lindahl, GROMACS: High performance molecular simulations through multi-level parallelism from laptops to supercomputers, SoftwareX 1 (2015) 19-25. https://doi.org/10.1016/j.softx.2015.06.001

[56] B. Hess. P-LINCS: a parallel linear constraint solver for molecular simulation, J. Chem. Theor. Comput. 4 (2008) 116-122. https://doi.org/10.1021/ct700200b

[57] U. Essmann, L. Perera, M. L. Berkowitz, T. Darden, H. Lee, L. G. Pedersen, A smooth particle mesh Ewald method, J. Chem. Phys. 103 (1995) 8577-8593. https://doi.org/10.1063/1.470117

[58] W. Humphrey, A. Dalke, K. Schulten, VMD: visual molecular dynamics, J. Mol. Graph. Model. 14 (1996) 33-38. https://doi.org/10.1016/0263-7855(96)00018-5

[59] E. F. Pettersen, T. D. Goddard, C. C. Huang, G. S. Couch, D. M. Greenblatt, E. C. Meng, T. E. Ferrin, UCSF chimera -A visualization system for exploratory research and analysis, J. Comput. Chem. 25 (2004) 1605-1612. https://doi.org/10.1002/jcc.20084

[60] B. G. Durie, W. S. Dalton, Reversal of drug-resistance in multiple myeloma with verapamil, Br. J. Haematol. 68 (1988) 203-206. https://doi.org/10.1023/A:1026556119020

[61] T. W. Sweatman, R. Seshadri, M. Israel, Metabolism and elimination of rhodamine 123 in the rat, Cancer Chemother. Pharmacol. 27 (1990) 205-210. https://doi.org/10.1007/BF00685714

[62] R. Yumoto, T. Murakami, M. Sanemasa, R. Nasu, J. Nagai, M. Takano, Pharmacokinetic interaction of cytochrome P450 3A-related compounds with rhodamine 123, a P-glycoprotein substrate, in rats pretreated with dexamethasone, Drug Metab. Dispos. 29 (2001) 145-151. PMID: 11159804

[63] Elodie Jouan 1, Marc Le V é e 1, Abdullah Mayati 1, Claire Denizot 2, Yannick Parmentier 2 and Olivier Fardel, Evaluation of P-Glycoprotein Inhibitory Potential Using a Rhodamine 123 Accumulation Assay, Pharmaceutics 2016, 8, 12; https://doi.org/10.3390/pharmaceutics8020012

[64] A. B. Ward, P. Szewczyk, V. Grimard, Structure of P-glycoprotein reveal its conformational flexibility and an epitope on the nucleotide-binding domain, Proc. Natl. Acad. Sci. U. S. A. 110 (2013) 13386-13391. https://doi.org/10.1073/pnas.1309275110

[65] P. H. Palestro, L. Gavernet, G. L. Estiu, L. E. B. Bruno, Docking Applied to the Prediction of the Affinity of Compounds to P-Glycoprotein, Biomed. Res. Int. 358425 (2014) 1-10. https://doi.org/10.1155/2014/358425

[66] T. W. Loo, D. M. Clarke, Identification of residues within the drug-binding domain of the human multidrug resistance P-glycoprotein by cysteine-scanning mutagenesis and reaction with dibromobimane, J. Biol. Chem. 275 (2000) 39272-39278. https://doi.org/10.1074/jbc.m007741200

[67] Mora Lagares L, Minovski N, Caballero Alfonso AY, et al. Homology Modeling of the Human P-glycoprotein (ABCB1) and Insights into Ligand Binding through Molecular Docking Studies. Int J Mol Sci. 2020; 21(11): 4058. Published 2020 Jun 5. https://doi.org/10.3390/ijms21114058

[68] T. W. Loo, M. C. Bartlett, D. M. Clarke, Identification of residues in the drug translocation pathway of the human multidrug resistance P-glycoprotein by arginine mutagenesis, J. Biol. Chem. 284 (2009) 24074-24087. https://doi.org/10.1074%2Fjbc.M109.023267

[69] E. Dolghih, C. Bryant, A. R. Renslo, M. P. Jacobson, Predicting binding to P-Glycoprotein by flexible receptor docking, Plos Comput. Biol. 7 (2011) e1002083. https://doi.org/10.1371/journal.pcbi.1002083

[70] S. Kanaoka, Y. Kimura, M. Fujikawa, Y. Nakagawa, K. Ueda, M. Akamats, Substrate recognition by P-glycoprotein efflux transporters: Structure-ATPase activity relationship of diverse chemicals and agrochemicals, J. Pestic. Sci. 38(2013) 112-122. https://doi.org/10.1584/jpestics.D13-022

[71] W. Liu, Q. Meng, Y. Sun, C. Wang, X. Huo, Z. Liu, P. Sun, H. Sun, X. Ma, K. Liu, Targeting P-Glycoprotein: Nelfinavir Reverses Adriamycin Resistance in K562/ADR Cells, Cell Physiol. Biochem. 51 (2018) 1616-1631. https://doi.org/10.1159/000495650

[72] L. Pan, S. G. Aller, Allosteric role of substrate occupancy toward the alignment of P-glycoprotein nucleotide binding domains, Sci. Rep. 8 (2018) 14643. https://doi.org/10.1038/s41598-018-32815-2

[73] S. G. Aller, J. Yu, A. Ward, Y. Weng, S. Chittaboina, R. Zhuo, P. M. Harrell, Y. T. Trinh, Q. Zhang, I. L. Urbatsch, G. Chang, Structure of P-glycoprotein reveals a molecular basis for poly specific drug binding, Science 323 (2009) 1718-1722. https://doi.org/10.1126/science.1168750

[74] Y. Raviv, H. B. Pollard, E. P. Bruggemann, I. Pastan, M. M. Gottesman, Photosensitized labeling of a functional multidrug transporter in living drug-resistant tumor cells, J. Biol. Chem. 265 (1990) 3975-80.
https://dx.doi.org/10.1016/S0021-9258(19)39690-5

Biography

Navanath Kumbhar is a Research Scholar at Department of Biotechnology, Medical Information Management, Shivaji University, Kolhapur, India. He has completed his doctoral work in Bioinformatics and Computational Biology in 2012, from Shivaji University Kolhapur. His expertise are conformational energy calculations of tRNA modifications using Semi-empircal PM6 and geometry optimizations using DFT, HF and MO6 methods were performed.. Homolegy modeling, molecular docking and MD simulations of P-glycoprotein (MDR), Synthetic iminosugars have been performed. The structural details of Fluorinated sugar amino acids peptides were predicted using DFT studies. subunit.

Rohit Bavi is a Postdoctoral Research Associate at China Pharmaceutical University. He has completed his doctoral studies from Shivaji University, Kolhapur in 2014. He is an expert in Schrodinger, Autodoc and structural biology.

Sagar Barage is an Associate Professor in Amity Institute of Biotechnology, Mumbai. He has completed his doctoral studies from Shivaji University, Kolhapur in 2014. His current research interest include Bioinformatics, Computational Biology, Drug designing, Molecular Modelling.

Ayesha Khan (nee Sabari Dutta) is an Assistant Professor in Savitribai Phule Pune University Department of Chemistry. She has completed her doctoral studies from Pune University. She has completed her postodoctoral research from School of medicine, Wayne State University, Michigan, USA. Her current research interest include Drug designing, Microbiology and animal tissue culture. Ms. Neelofar Khan was a Project Assistant at Institute of Bioinformatics and Biotechnology who synthesized the esculetin compounds.